Available online at www.sciencedirect.com
SCIENCE DIRECT®
Journal of Fluorine Chemistry 120 (2003) 157–163
JOURNAL OF FLUORINE CHEMISTRY
www.elsevier.com/locate/jfluchem

Fabrication of high performance thin films from metal fluorocomplex aqueous solution by the liquid phase deposition

Hnin Yu Yu Ko[a], Minoru Mizuhata[b], Akihiko Kajinami[b], Shigehito Deki[b,*]

[a]*Department of Chemistry, School of Science and Technology, Kwansei Gakuin University, 2-1 Gakuen, Sanda, Hyogo 669-1337, Japan*
[b]*Department of Chemical Science and Engineering, Faculty of Engineering, Graduate School of Science and Technology, Kobe University, Rokkodai, Nada, Kobe 657-8501, Japan*

Received 1 August 2002; received in revised form 7 October 2002; accepted 11 October 2002

Abstract

The hetro-structured oxide thin films from metal fluorocomplex solution have been prepared by the liquid phase deposition (LPD) method. The Pt/Nb_2O_5 and Au/Nb_2O_5 composite films can be prepared from a mixed solution of niobium source, H_3BO_3, $Pt(NH_3)_4Cl_2$ and $HAuCl_4$ aqueous solutions under the ambient temperature and atmosphere. In the case of Au/SiO_2 composite film, $(NH_4)_2SiF_6$ solution is used as a mother solution. The Pt and Au ionic species are deposited in Nb_2O_5 and SiO_2 matrices. They are reduced to their metallic state after treatment above 200 °C. The size of dispersed particles can be controlled by heat treatment temperature. It is also clear that, gold nanoparticles are also found to interact with SiO_2, although the interaction is smaller than that with Nb_2O_5 showing the size of Au nanoparticles remain smaller in Nb_2O_5 that in SiO_2.

Keywords: Synthesis; Nanoparticles; Liquid phase deposition; Metal oxide; Thin film; Hetro-structure

1. Introduction

Nano-sized noble metal particles, because of their surface and quantum-size effects, display many novel properties, such as high catalytic activities, non-linear optical properties, and various properties from a fundamental viewpoint. In the materials for the production of non-linear optical devices, it is important to ensure a layer or circuit pattern. The use in a practical application, however, imposes on these materials quite severe restrictions concerning accurate control of the particles: distribution, shape, dimensions and homogeneity.

Accordingly, considerable effort has been focused on the development of synthetic techniques. Actually, the composite films have been fabricated using various methods, such as rf sputtering, ion-implantation, and sol–gel method [1–3]. The liquid phase deposition (LPD, also known as chemical bath deposition) method which has been developed and reported previously is a wet process employed to prepare metal oxide thin films from aqueous solutions as low temperatures (30–50 °C) [4,5]. Compared to vapor deposition techniques, the LPD method offers lower capital equipment costs (based on aqueous precursors), energy efficiency, and flexibility in the choice of substrates with respect to topography and thermal stability with large surface area. The obtained films are particularly stable compared with films prepared by the other non-vacuum techniques. This method is also used to incorporate dopants in thin films as precisely as possible.

The LPD process utilizes ligand-exchange hydrolysis of metal fluorocomplex species, $MF_x^{(x-2n)-}$ and F^- consumptive reaction. In aqueous solution, $MF_x^{(x-2n)-}$ is hydrolysed with water following ligand-exchange equilibrium reaction:

$$MF_x^{(x-2n)-} + nH_2O = MO_n + xF^- + 2nH^+ \quad (1)$$

This reaction can be shifted to the right-hand side by adding boric acid or aluminum metal, which reacts with F^- ions to form more stable complex ions:

$$H_3BO_3 + 4HF = BF_4^- + H_3O^+ + 2H_2O \quad (2)$$

$$Al + 6HF = H_3AlF_6 + \tfrac{3}{2}H_2 \quad (3)$$

The addition of the boric acid or aluminum metal leads to the consumption of F^- ions and accelerates the ligand-exchange reaction. Thus, thin films are slowly deposited homogeneously on the substrates. So far, we have already developed and reported the preparation of various kinds of metal oxide

* Corresponding author. Tel.: +81-78-803-6160; fax: +81-78-803-6160.
E-mail address: deki@kobe-u.ac.jp (S. Deki).

0022-1139/02/$ – see front matter
PII: S0022-1139(02)00325-1

thin films such as titanium oxide [6], vanadium oxide [7], iron oxide [8], gradient-type $Si_{1-x}Ti_xO_2$ [9], and so on [10] by the LPD method.

In this paper, we describe the fabrication and characterization of hetro-structured oxide such as Au and Pt nanoparticles-dispersed Nb_2O_5 or SiO_2 composite films by the LPD method. The characteristics of the deposited films are discussed on the basis of results obtained from X-ray diffraction (XRD), high-resolution transmission electron microscopy (HRTEM), X-ray photoelectron spectroscopy (XPS) and Fourier transform infrared spectroscopy (FT-IR).

2. Results and discussion

The deposited films are transparent, of uniform thickness and appearance, and adhere strongly to the substrates. The color of composite films has changed according to those of the heat treatment temperature. In the Au/Nb_2O_5 system, the as-deposited film (before heat treatment) has a pale yellow, and gradually changed to deep yellow at 100 °C, a white blue at 200 °C, deep blue color at 300 °C and above, respectively. For the Au/SiO_2 system, the composite film changed light yellow to ruby red color after treatment at 300 °C. In the case of Pt/Nb_2O_5 system, the composite film slightly changed a pale yellow to brown color with increasing treatment up to 600 °C. These color changes are indicative of the formation of Au and Pt particles in the composite films. The thicknesses after treatment at 500 °C are about 100 nm for Au/SiO_2, 80 nm for Pt/Nb_2O_5, and 150 nm for Au/Nb_2O_5 composite films, respectively.

2.1. Au nanoparticles dispersed-Nb_2O_5 composite film

FT-IR spectra of the Au/Nb_2O_5 composite films with various heat treatment temperatures are shown in Fig. 1 by emphasizing the regions of changes with arrows. All deposited films show the main bands at 650–1000 cm^{-1} which are attributed to Nb–O stretching, Nb–O–Nb bridging and Nb_3–O stretching modes. The bands at 1400 and 1540 cm^{-1}, and a broad one at 2800–3700 cm^{-1} are assigned to the O–H and N–H vibrations for water molecules and NH_4^+ ions, respectively [11]. Since the LPD process is performed in an aqueous solution system, water molecules can be readily absorbed and adsorbed by the film. NH_4^+ ions which are contained in the niobium source solution are enclosed in the deposited oxide film during the reaction. These O–H and N–H vibration bands completely disappear after treatment above 200 °C.

The Au 4f, Nb 3d, O 1s, F 1s, and N 1s core-level spectra for the deposited films with various heat treatment temperatures are shown in Fig. 2. These spectra are recorded at room temperature. For the Au 4f electron spectra show the typical doublet structure (Au $4f_{5/2}$ and Au $4f_{7/2}$) due to spin–orbit splitting. From the curve-fitting result of the as-deposited

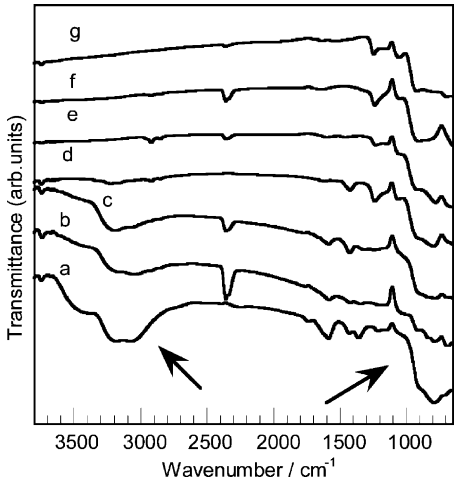

Fig. 1. FT-IR spectra of the Au/Nb_2O_5 composite films heat-treated at various temperatures: (a) as-deposited film, and (b–g) films heat-treated at 100–600 °C, respectively.

film, the Au $4f_{7/2}$ peak positioned at 86.9 eV assigning to Au(III) ionic state [12]. After heating at 100 °C, this peak shifted to lower energy side as compared to that of as-deposited film indicating Au(I) ionic state. The fitting of Au 4f exhibit two binding energies for Au $4f_{7/2}$ at 86.9 and 86.0 eV representing Au(III) and Au(I) ionic states, respectively. For the films treated at 200 °C, the spectra become sharpened and the Au $4f_{7/2}$ peaks are observed near 84.0 eV assigning to metallic Au (Au^0).

The reduction Au ionic species may not occur without the decomposition of $AuCl_4^-$ ionic species. Therefore, it is considered that $AuCl_4^-$ ionic species are decomposed between 100 and 200 in the airflow as follows:

$$AuCl_4^- \rightarrow Au + \tfrac{3}{2}Cl_2 + Cl^- \quad (4)$$

Au atoms produced by the decomposition of $AuCl_4^-$ should tend to aggregate to form nanocrystal.

$$nAu^0 \rightarrow (Au^0)n \quad (5)$$

In the case of Nb 3d peaks, for the as-deposited film, a pair of peaks due to Nb $3d_{3/2}$ and Nb $3d_{5/2}$ core-level is observed at the binding energies of ca. 211.3 and 208.5 eV. The Nb $3d_{5/2}$ peak position states a higher energy than that of the bulk Nb_2O_5 (207.8 eV). The electron spectra of F 1s and N 1s are also observed at ca. 685.0 and 401.0 eV, respectively. The O 1s electron spectra show broad and asymmetrical profiles which may be connected with the presence of hydroxyl groups and adsorbed water molecule [13]. However, these peaks become sharp with increasing heat treatment temperature. It indicates the elimination of water from the film due to the treatment. The corresponding O 1s peaks of all the deposited films are centered on 530.5 eV and can be assigned to the O^{2-} constituent of the Nb_2O_5.

The LPD process performs typical aqueous solution system, and it may be contained water molecule in the deposited film. Moreover, a small trace of ammonia ions

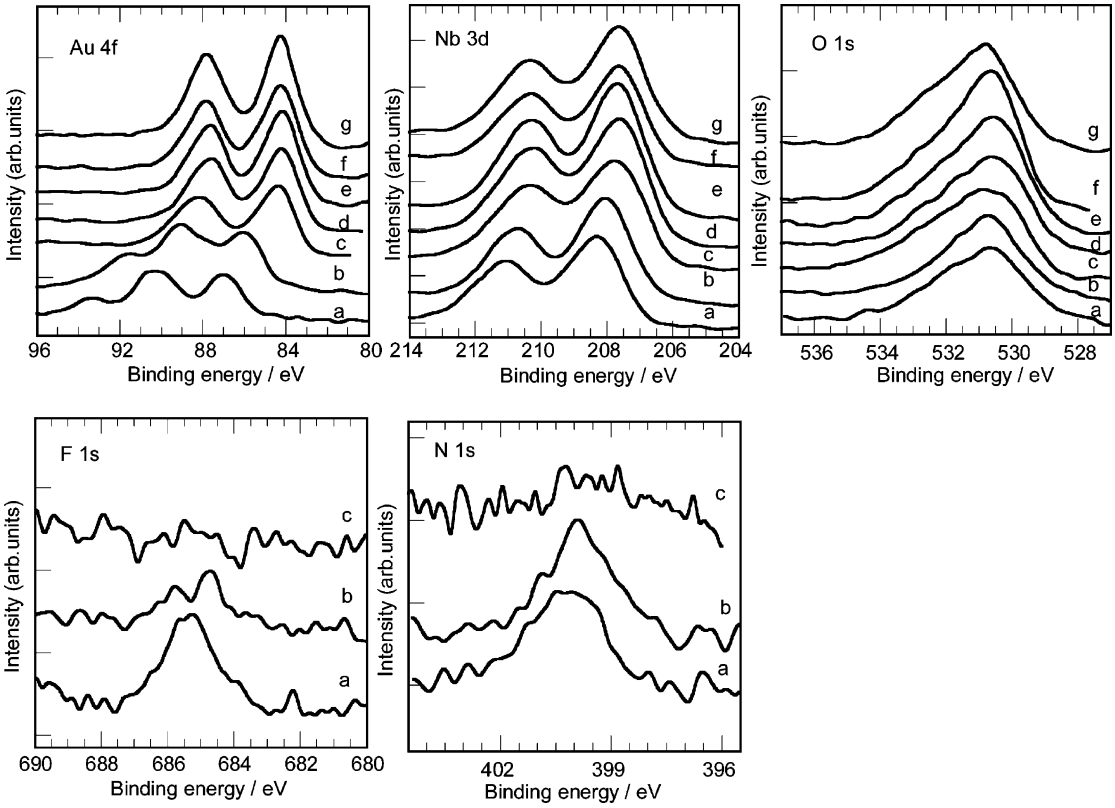

Fig. 2. Evolution of the Au 4f, Nb 3d, O 1s, F 1s, and N 1s electron spectra of the Au/Nb_2O_5 composite films heat-treated at various temperatures: (a) as-deposited film, and (b–g) films heat-treated at 100–600 °C, respectively.

may also be existed in the deposited film because of using the source material (Nb_2O_5 dissolved $NH_4F{\cdot}HF$ aqueous solution) for the thin film formation process. From the changes of Nb 3d, O 1s, F 1s, and N 1s spectra with heat treatment temperature, it can be considered that interactions such as Nb–F, Nb–OH, and Nb–OF exist in the as-deposited film. The disappearance of F 1s, N 1s peaks, and sharpening of O 1s peak with the increase of heating are indicated that the elimination of fluorine, nitrogen and water from the deposited film. Further gradually increase up to 600 °C, the Nb $3d_{5/2}$ and O 1s peaks were ca. 207.7 and 530.2 eV, respectively, corresponding to that of bulk Nb_2O_5. These energies are in good agreement with the other study [14].

2.2. Au nanoparticles dispersed-SiO_2 composite film

The deposited Au/SiO_2 composite films are constructed of small particles and very homogeneous, showing no crack and exfoliation. The small particles become large by heat treatment. From the FT-IR measurement, Si–O stretching (1090 cm^{-1}), Si–O bending (810 cm^{-1}) modes are observed [15]. We can confirm these absorption peaks for all composite films before and after heat treatment. XPS profile indicates that Au(III) ionic species are deposited in the as-deposited film. Au ionic species in the composite film are completely reduced to metallic Au (Au^0) by the treatment above 200 °C. Therefore, the reduction mechanism for Au ionic species can be considered the same as Au/Nb_2O_5 composite film system.

2.3. Micro-structure of Au/Nb_2O_5 and Au/SiO_2 composite films

Fig. 3 shows a comparison of the X-ray diffraction pattern of the Au/Nb_2O_5 and Au/SiO_2 composite films with before and after heat treatment at 500 °C. There is no distinct diffraction peak, which indicates that Nb and Si oxides have amorphous structure (Fig. 3a and b). As considered from the Scherrer's equation, the broader the peak becomes, the smaller the crystal grows. For the composite films treated at 500 °C, the two sharp diffraction peaks at ca. $2\theta = 38.1$ and 44.4° attributed to (1 1 1) and (2 0 0) reflections of Au with an fcc structure are observed (shown with white circles in the figure). These two diffraction peaks become much shaper in the pattern of Au/SiO_2 film while in those of Au/Nb_2O_5 composite film remains broad. The crystallite sizes calculated by Scherrer's equation for the diffraction line from Au(1 1 1) and the mean sizes of dispersed Au particles are estimated by plan-view TEM observation are summarized in Table 1. Gold particles grow into large aggregates in the heat-treated Au/SiO_2 composites [16]. However, in the Au/Nb_2O_5 composite film, even after treated at high temperature, the Au crystallite size remains very small. Moreover, at 500 °C, the new diffraction peaks appear at ca.

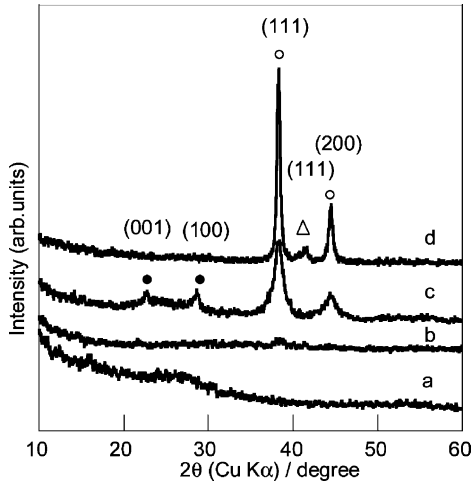

Fig. 3. XRD patterns of the deposited films: as-deposited Au/Nb_2O_5 (a), that of Au/SiO_2 (b), film heat-treated at 500 °C Au/Nb_2O_5 (c), and that of Au/SiO_2 composite films (d), respectively. (○) Au; (●) Nb_2O_5, (△) Si (substrate).

$2\theta = 22.6$ and 28.6° due to the hexagonal TT-Nb_2O_5 phase (shown with black circles in the Fig. 3c) (JCPDS 28-317 data.). The TT phases are named by German workers and signified the low- (tief) and very low-temperature (tief–tief) forms of Nb_2O_5 [17].

The cross-sectional HRTEM observation of heat-treated Au/Nb_2O_5 (600 °C, 1 h) and Au/SiO_2 (300 °C, 1 h) composite films are shown in Fig. 4. It can be clearly observed that the dark patches, Au particles are homogeneously dispersed into the Nb_2O_5 and SiO_2 matrices. Au nanoparticles are uniformly situated not only on the surface but also inside of the composite film. Lattice fringe corresponding to Nb_2O_5(0 0 1) plane are observed with the spacing of 0.41 nm and the Nb_2O_5 nanocrystalline particles (ca. 10 nm) are situated all over the composite film. It can be clarified that not only Au ionic species are reduced to Au metal particles but also Nb_2O_5 matrix is crystallized by the heat treatment.

2.4. Optical properties of Au/Nb_2O_5 and Au/SiO_2 composite films

Fig. 5 shows the optical absorption spectra of the Au/Nb_2O_5 and Au/SiO_2 composite films with before and after heat treatment at 500 °C. In both cases of as-deposited films, the surface plasmon resonance (SPR) peaks of Au particles are not discernible. In the heat-treated samples, the SPR peaks of Au particles are observed at 550 and 580 nm for Au/SiO_2 and Au/Nb_2O_5 composite films, respectively. The

Table 1
Crystallite and mean particle sizes of the dispersed Au metal particles in the composite films heat-treated at various temperatures

	Heat-treatment temperature (°C)	Crystallite size (nm)	Mean particle size (nm)
Au/Nb_2O_5	300	8.0	7.0
Au/SiO_2	300	11.0	10.5
Au/Nb_2O_5	500	10.0	9.5
Au/SiO_2	500	16.5	16.0

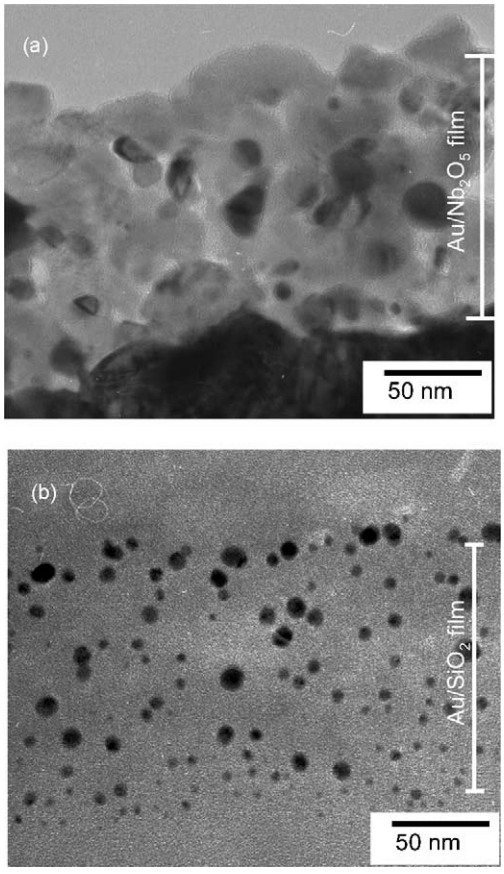

Fig. 4. Cross-sectional HRTEM images of the deposited composite films: (a) Au/Nb_2O_5 (600 °C, 1 h), and (b) Au/SiO_2 (300 °C, 1 h), respectively.

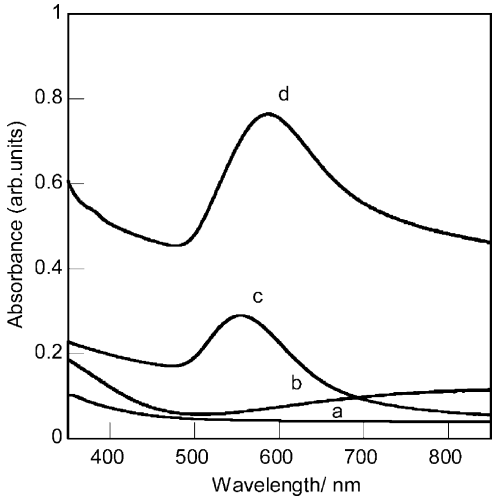

Fig. 5. Optical absorption spectra of the deposited films: as-deposited Au/SiO_2 (a), that of Au/Nb_2O_5 (b), and film heat-treated at 500 °C Au/Nb_2O_5 (c), and that of Au/SiO_2 composite films (d), respectively.

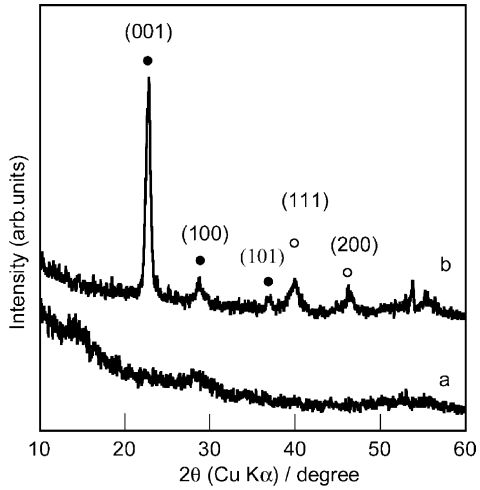

Fig. 6. XRD patterns of the Pt/Nb_2O_5 composite films: (a) as-deposited film, and (b) film heat-treated at 600 °C, respectively. (○) Pt; (●) Nb_2O_5.

surface plasmon resonance of Au nanoparticles is greatly affected by the surrounding metal oxides. We assume that strong interactions exist between oxide and gold, which causes the oxide to surround gold nanoparticles and keep them from aggregating. It is reported that small particles are known to interact well with transition metal oxides and very weak interaction with non-transition metal oxides [18,19]. In this study, gold nanoparticles are also found to interact with SiO_2, a non-transition metal oxide, although the interaction is smaller than that with Nb_2O_5, because Au nanoparticles remain smaller in Nb_2O_5 than in SiO_2.

The plasmon band is affected by the volume fraction and micro-structures of the embedded metal clusters, together with the dielectric constant of the matrix. These are key factors to control the optical properties of metal nanoparticles [20,21]. In our study, the red shift of SPR peaks is observed in the Au/SiO_2 and Au/Nb_2O_5 composite films casing particle size effect with increasing treatment temperature.

2.5. *Pt nanoparticles dispersed-Nb_2O_5 composite film*

X-ray diffraction patterns of the Pt/Nb_2O_5 composite films, as-deposited and heat-treated at 600 °C are shown in Fig. 6. The deposited films exhibit amorphous nature, i.e. no discernible diffraction peaks are observed up to 500 °C. After at 600 °C, the diffraction peaks (indicating the crystallinity) appear approximately at $2\theta = 22.6$, 28.6 and 36.8° (shown with black circles in the figure) assigned to the hexagonal TT-Nb_2O_5 phase (JCPDS 28-317 data). Furthermore, the two sharp diffraction peaks are observed approximately at $2\theta = 39.8$ and 46.4° (shown by white circles in the figure) attributed to (1 1 1) and (2 0 0) reflection lines of the cubic structure of Pt, respectively.

XPS are measured for Pt 4f electron band of the composite films as a function of heat treatment temperatures. For the

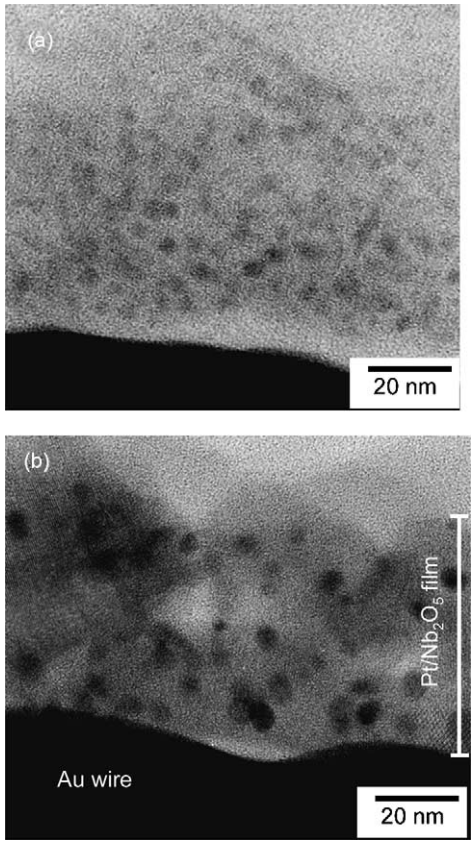

Fig. 7. Cross-sectional HRTEM images of the Pt/Nb_2O_5 composite films deposited on gold wire: (a) as-deposited film, and (b) film heat-treated at 300 °C, respectively.

as-deposited film, the Pt $4f_{7/2}$ peak is observed at 72.6 eV and assigned to Pt(II) ionic state. This indicates that the Pt is situated in the niobium oxide matrix as ionic state in the as-deposited film. The peak position of Pt $4f_{7/2}$ shifts to the lower energy side with increasing temperatures. At 300 °C, Pt 4f peak separates into two binding energies for Pt $4f_{7/2}$ peaks at 72.6 and 71.2 eV standing for Pt(II) ionic state and metallic Pt (Pt^0) state, respectively [22]. For the films treated at 500 °C, the Pt $4f_{7/2}$ peaks are observed near 71.0 eV. Therefore, the partial reduction of Pt(II) ionic species in the deposited films is expected to be observed after being treated at 200 °C and the complete reduction may be occurred about 500 °C.

Fig. 7 shows the cross-sectional HRTEM images of the Pt/Nb_2O_5 composite films, as-deposited and heat-treated at 600 °C. The as-deposited film exhibits an amorphous nature (Fig. 7a). This result is good agreement with that of XRD result (Fig. 6a). In contrast, the spherical Pt particles are homogeneously dispersed into the Nb_2O_5 matrix after treatment at 600 °C (Fig. 7b). The size of Pt particles (with mean sizes of 2–6 nm) dispersed in the film are mostly single crystal and distributed around the Nb_2O_5 nanocrystalline particles. The Nb_2O_5 nanocrystalline particles (nearly 10 nm) are observed throughout the entire deposited film. These results signify that the heat treatment not only causes

the reduction of Pt(II) ionic species to Pt particles but also involves the crystallization of Nb_2O_5 matrix.

3. Experimental

3.1. Preparation of Au and Pt nanoparticles dispersed-Nb_2O_5 and SiO_2 composite films

As the niobium source solution for deposition of Nb_2O_5 film, niobium(V) oxide (Nb_2O_5; Taki Chemical Co. Ltd.) powder and $NH_4F{\cdot}HF$ (Nacalai Tesque Inc.) aqueous solution were used. This solution was obtained by dissolving Nb_2O_5 powder (7.4 g, 20 mmol) in $NH_4F{\cdot}HF$ (57.9 g, 1.0 mol) aqueous solution (1000 ml). For deposition of SiO_2 film, ammonium siliconhexafluoride acid ($(NH_4)_2SiF_6$) was employed. The boric acid (H_3BO_3) was used as a F^- scavenger. As platinum and gold precursors, Tetra-ammineplatinum chloride ($Pt(NH_3)_4Cl_2$) and tetra-chloroauric ($HAuCl_4{\cdot}4H_2O$)acid solutions were prepared.

Various substrates were employed depending on the needs of the different characterization techniques. The non-alkali glass (corning 7059) and Si(1 1 1) wafers were used as substrates for the XPS, FT-IR and XRD measurements. For the HRTEM cross-sectional observation, the composite films were deposited on gold wire. After being degreased and washed ultrasonically, the substrates were vertically placed in a freshly prepared solution containing 4.0 mM (1 M = mol dm^{-3}) niobium source solution, 0.2 M H_3BO_3, 0.4 mM $HAuCl_4{\cdot}4H_2O$ for Au/Nb_2O_5 composite film and 0.6 mM $Pt(NH_3)_4Cl_2$ for Pt/Nb_2O_5 composite film, were kept 30 °C for 40 h. They were then removed and washed with deionized water. After that the samples were dried in ambient temperature. The deposited films were pre-treated at 100–600 °C in airflow for 1 h before being removed for spectroscopic and microscopic observations. For the preparation of Au/SiO_2 composite films, 0.1 M $(NH_4)_2SiF_6$, 0.2 M H_3BO_3, and 0.4 mM $HAuCl_4{\cdot}4H_2O$ were used with the same manner under 40 °C for 48 h.

3.2. Characterization of the deposited composite films

The phases and the crystallographic structures of the deposited films were determined by XRD measurement on Rigaku RINT-2100 diffractometer equipped with a thin film attachment using Cu Kα radiation. The incident angle of the X-ray to the sample was 1°. XPS analyses were carried out in a KRATOS, XSAM 800 with Mg Kα radiation (1253.6 eV) for the determination of the oxidation state and the chemical structure of materials. The C 1s peak (284.6 eV) was used as reference for the correction of the XPS positions of the obtained films. TEM images, which were obtained using a JEOL JEM-2010 at acceleration voltage of 200 kV, were used to observe the morphology and size of particles in the composite films. The preparation of the cross-sectional HRTEM observation is expressed detail in the [10]. The infrared spectra of the films were recorded with a FT/IR615 (JASCO) spectrometer equipped with a RAS attachment (PR-510, JASCO) in the range of 650–3650 cm^{-1}. The resolution and incident angle were 2 cm^{-1} and 65°, respectively.

4. Conclusions

We have developed a very simple soft solution process for fabrication of hetro-structured oxide thin films from metal fluorocomplex aqueous solution such as Au and Pt nanoparticles-dispersed metal oxide (M = Nb or Si) thin films. The Nb_2O_5 thin films containing Pt, Au ionic species are deposited from a mixed solution of niobium source, H_3BO_3, $Pt(NH_3)_4Cl_2$ and $HAuCl_4$ aqueous solutions under the ambient temperature and atmosphere. For Au/SiO_2 composite film, $(NH_4)_2SiF_6$ solution is used as a mother solution. The Pt(II) and Au(III) ionic species are deposited in Nb_2O_5 and SiO_2 matrices. They are reduced to their metallic state after treatment above 200 °C. All deposited films are X-ray amorphous up to treatment of 500 °C, above of which the hexagonal structure of TT-Nb_2O_5 are observed although silica is still amorphous. The dispersion of particles in the matrices is homogeneous. The size of dispersed particles can be controlled by heat treatment temperature. It is also clear that, gold nanoparticles are also found to interact with SiO_2, although the interaction is smaller than that with Nb_2O_5 showing the size of Au nanoparticles remain smaller in Nb_2O_5 that in SiO_2. The LPD method enables us to form nanoscale structure in solid dielectric materials, in which the fine structures such as size and concentration of dispersed metal particles.

Acknowledgements

This work was partly supported by Grants-in-Aid for Scientific Research No. 12305056 from the Ministry of Education, Science, Sports and Culture, Japan.

References

[1] T. Kineri, M. Mori, K. Kadono, T. Sakaguchi, M. Miya, H. Wakabayashi, T. Tsuchiya, J. Ceram. Soc. Jpn. 101 (1993) 1340–1343.
[2] K. Fukumi, A. Chayahara, K. Kadono, T. Sakaguchi, Y. Horino, M. Miya, K. Fujii, J. Hayakawa, M. Satou, J. Appl. Phys. 75 (6) (1994) 3075–3080.
[3] H. Yanagi, S. Mashiko, L.A. Nagahara, H. Tokumoto, Chem. Mater. 10 (1998) 1258–1264.
[4] H. Nagayama, H. Honda, H. Kawahara, J. Electrochem. Soc. 135 (1988) 2013–2015.
[5] A. Hishinuma, T. Goda, M. Kitaoka, S. Hayashi, H. Kawahara, Appl. Surf. Sci. 48 (49) (1991) 405–408.
[6] S. Deki, Y. Aoi, O. Hiroi, A. Kajinami, Chem. Lett. 6 (1996) 433–434.

[7] S. Deki, Y. Aoi, A. Kajinami, J. Mater. Sci. 32 (1997) 4269–4273.
[8] S. Deki, Y. Aoi, J. Okabe, H. Yanagimoto, A. Kajinami, M. Mizuhata, J. Mater. Chem. 7 (9) (1997) 1769–1772.
[9] S. Deki, S. Iizuka, K. Akamatsu, M. Mizuhata, A. Kajinami, J. Mater. Chem. 11 (2001) 1–4.
[10] H.Y.Y. Ko, M. Mizuhata, A. Kajinami, S. Deki, J. Mater. Chem. 12 (2002) 1495–1499.
[11] M. Macek, B. Orel, U.O. Krasovec, J. Electrochem. Soc. 28 (1983) 17–20.
[12] J.J. Pireaux, M. Liehr, P.A. Thiry, J.P. Caudano, Surf. Sci. 141 (1984) 221–232.
[13] V.P. Poroshkov, V.S. Gurin, Surf. Sci. 331–333 (1995) 1520–1525.
[14] E.I. Ko, J.G. Weissman, Catal. Today 8 (1990) 27–36.
[15] R.J. Davis, Z. Liu, Chem. Mater. 9 (1997) 2311–2316.
[16] S.C. Davis, K.J. Klabunde, Chem. Rev. 82 (1982) 153–208.
[17] J.G. Weissman, E.I. Ko, P. Wynblatt, J. Catal. 108 (1987) 383–400.
[18] M.G. Mason, Phys. Rev. B 27 (1983) 748–762.
[19] S.J. Tauster, S.C. Fung, R.L. Garten, J. Am. Chem. Soc. 100 (1978) 170–175.
[20] R.H. Doremus, J. Chem. Phys. 40 (1964) 2389–2396.
[21] U. Kreibig, L. Ganzel, Surf. Sci. 156 (1985) 678–700.
[22] M. Peuckert, H.P. Bonzel, Surf. Sci. 145 (1984) 239–259.